Theor Chem Acc (2012) 131:1228
DOI 10.1007/s00214-012-1228-5

REGULAR ARTICLE

Ab initio investigation of the structural stability and optical properties of low-density amorphous carbon doped with N, B, and Fe

Charles W. Bauschlicher Jr. · John W. Lawson

Received: 21 March 2012 / Accepted: 21 April 2012 / Published online: 13 May 2012

Abstract The addition of iron or boron and/or nitrogen, up to 20 %, to amorphous carbon with a density of about 2.0 gm/cm^3 was studied using density functional theory. The bulk cohesive energy decreases with increasing iron, nitrogen, or boron concentration. The decrease is largest for iron and smallest for boron. The trends in the bulk moduli are consistent with the cohesive energies. The optical properties (absorbance and reflectivity) of the samples with nitrogen and/or boron added are very similar to those of the original amorphous carbon. Addition of iron results in larger, energy dependent, changes when compared with either boron or nitrogen. The effect of dopants on low-density amorphous carbon shows some differences with those for higher density amorphous carbon.

Keywords Amorphous carbon · DFT · Surfaces · Dopants · Cohesive energy · Optical properties

1 Introduction

Amorphous carbon has been the subject of numerous studies recently (see for example [1–16]). While many empirical approaches have had considerable success, the best agreement with experiment is obtained using density functional theory (DFT) (see the reviews by Robertson [11] and McKenzie [16]). There has also been investigations of the effect of dopants on amorphous carbon: Fe (see for example references [17–21]), nitrogen (see for example references [22–39]) and boron (see for example references [40–46]). Most of this previous work has focused on higher density (2.6–3.2 g/cm^3) amorphous carbon, where the carbon–carbon bonding is dominated by sp^3 carbons. In these studies, it was concluded that adding Fe, N, or B atoms caused the isolated pairs of sp^2 bonded carbons to form more extended networks of sp^2 bonded carbons. On the basis of Raman spectra, one study [18] even suggested that the sp^2 network was in the form of carbon nanotubes. These extended sp^2 networks increase the absorption in the 0–8 eV range.

While the experiments on these materials have yielded a lot of interesting information, they may be difficult to interpret; for example, Kalijadis et al. [46] found that adding boron chemically did not change the surface hardness, while adding it by ion implantation significantly increased the hardness. Because they added the boron in two ways, they were able to conclude that the energy associated with the ion impact increased the carbon–carbon bonding and changed the hardness, that is, the addition of the boron was not a significant factor. Because of the difficulty in interpreting experiments, it is not surprising that many computational studies have been performed to obtain an understanding of these materials.

Low-density amorphous carbon is used in ablative thermal protection systems (TPS) for space vehicles during atmospheric entry. These materials are commonly fiber materials with a low-density polymer matrix that pyrolyzes into an amorphous carbon char under the intense convective and radiative heating conditions. Radiative heating does not occur in many TPS applications, but can be more than half of the total instantaneous heating for some

C. W. Bauschlicher Jr. (✉)
Entry Systems and Technology Division, Mail Stop 230-3, NASA Ames Research Center, Moffett Field, CA 94035, USA
e-mail: Charles.W.Bauschlicher@nasa.gov

J. W. Lawson
Thermal Protection Materials Branch, Mail Stop 234-1, NASA Ames Research Center, Moffett Field, CA 94035, USA
e-mail: John.W.Lawson@nasa.gov

high-speed atmospheric entries. The properties of this char (thermal stability, response to radiation, etc) are important to determine the overall performance of the TPS. The presence of non-carbon species are also expected to affect performance. These additions may be intentional to improve particular properties or they may be impurities introduced during processing that will degrade performance. In either case, understanding the effect of dopants/impurities on low-density amorphous carbon is important for further material development and evaluation of material performance.

Amorphous carbon with a density of 2.0 g/cm^3 has some C–C bonds where the bond length is stretch or the bond angle distorted compared the ideal case [1]. Replacing the carbon atoms with the strained bonds with a B or a N atom might remove the strained bond, and, after relaxation, the overall bonding might be improved. Alternatively adding an atom, such as Fe, that can form more than four bonds and has greater flexibility in the optimal bond angles could improve the bonding. The higher density studies have shown that B, N, and Fe affect the pi network and supports the idea that these atoms might change the properties at lower densities as well. Therefore, we consider B, N, and Fe as dopants/impurity atoms.

Previous studies have focused on these impurities in high density amorphous carbon, whereas for TPS entry applications, low-density carbon is of primary interest. In our previous study [1], we found that amorphous carbon with a density of 2.0 g/cm^3 is dominated by extended sp^2 bonding while higher density (2.6–3.2 g/cm^3) is dominated by the sp^3 bonding with only isolated sp^2 bonding. This change in the bonding with density means that it is not easy to extrapolate the previously deduced effect of dopant on higher density amorphous carbon to lower densities and therefore simulations including Fe, B, and/or N dopant atoms need to be performed on lower (2.0 g/cm^3) density amorphous carbon. We use the DFT approach that has been shown to be the most reliable for the pure carbon and the mixed systems are likely to be more complex than pure carbon. In addition to bulk properties, like cohesive energy, bulk modulus, and optical properties, we also perform some investigation of surface properties, because even if addition of dopants does not improve the bulk properties, the dopants could result in additional bonds between the existing sp^2 bonding networks and therefore strengthen surface of the lower density char.

2 Methods

This work uses the same protocol as in our recent density functional theory (DFT) based study [1] of amorphous carbon. In simulations of the bulk, the number of atoms and the density determine the cell size, which, for convenience, is chosen to be a cube. We use 64 atoms in all of our simulations. Our cube size is determined for a carbon density of 2.00 g/cm^3. Replacing a few carbon atoms with a few boron or nitrogen atoms without changing the cell size changes the density slightly. Since the change in density is small, we do not change the cell size when boron or nitrogen atoms are added. Iron has a much larger mass than carbon, and changing only six carbon atoms to iron atoms yields a density of 2.7 g/cm^3. Therefore, in the iron case both the fixed cell size (i.e., fixed volume) and fixed density (2.00 g/cm^3) simulations are performed.

We add 64 atoms to the cell at random coordinates; the addition of an atom is rejected if it is within 1.1 Å of any of the existing atoms. For the simulations with n dopant atoms, from the list of 64 atomic positions, n are selected at random and assigned as dopant atoms. These random positions are randomized further by performing DFT-based molecular dynamics simulations for 1 ps at 5,000 K. Previous work on pure carbon systems shows that these geometries are similar to those obtained from molecular dynamics simulations for 1 ps at 5,000 K starting from a regular lattice of carbon atoms. However, the random approach allows the formation of local minima if a lower initial temperature is used. Such local minima are not considered in this work. The system is quenched from 5,000 to 0 K in 4 ps; the temperature is reduced linearly during the quench. The geometry is then optimized at 0 K.

For selected systems, we varied cell size, optimizing the atomic positions for each choice of cell size. The energy versus volume was fit to a parabolic function and used to compute the bulk modulus at 0 K. While this procedure worked for most simulations, in a few cases, the change in cell size lead to a lower energy solution. In those cases, the lower energy solution was used as a new equilibrium geometry and the process repeated.

For the studies of the surfaces, we start from the geometries obtained in the bulk calculations, change one dimension of the cell, center the slab in the expanded cell direction, and optimize the atomic positions in the slab calculations. Thus two of the dimensions are taken from the bulk, while the third dimension is made sufficiently large that the neighboring slabs do not interact. We compute the density in the surface calculations using the positions of the upper and lower most atom in the surface direction and the cell sizes in the periodic directions. This approach is perhaps a bit simplistic, however, we believe that it is sufficiently consistent that we can compare different surfaces and look for trends. For the surface calculations, the initial relaxation is 1 ps at 700 K, followed by 1 ps quenching from 700 to 0 K, and by a 0 K optimization.

To determine the bulk optical absorption properties, the ion-clamped frequency-dependent real and imaginary

dielectric functions are computed using density functional theory in conjunction with the RPA approximation [47, 48]. DFT may not give accurate optical spectra because in general it does not give a good description of excited states. However, we are interested in relative differences, and therefore this approach should be adequate. While the cell is cubic, the amorphous nature of the systems means that the x, y, and z components are different, therefore, we report the sum of x + y + z.

In addition to the optical properties, the site-projected density of states (DOS) are computed. The Bader method is used to define the atomic volumes [49]. In this approach, the dividing surfaces are at minima in the electron density; this is expected to be more accurate than a simple spherical shell about each atom. However, even for this approach, the sum of the site-projected DOSs does not agree with the total DOS, but the difference is sufficiently small that the site-projected DOS curves can be used to understand the effect of the dopant atoms.

All of the calculations are performed using the Vienna ab initio simulation package (VASP), version 5.2 or earlier [50–53]. The generalized gradient corrected functional of Perdew and Wang [54] is used. We use a plane wave basis set in conjunction with the projector augmented wave method [55] (PAW). For iron the 8 valence electron PAW is used, because preliminary studies showed that the results of the 8 and 16 valence electron PAWs are very similar. In the 0 K calculations, a plane wave cutoff of 400 eV is used, while for the molecular dynamics calculations, a lower cutoff of 300 eV is used. On the basis of our previous study of carbon char [1], a sampling of k-space at the Γ point is sufficient.

We used molecular dynamics only to generate structures using the melt-and-quench algorithm, which was followed by energy minimization. We expect time step errors to be minimal for a range of choices of time step and quench time and this was confirmed in a series of tests [1, 13]. Our choice of a 2 fs time step in conjunction with a 4 ps quench is a conservative choice as a 3 fs time step with a 2 ps quench gave structures with no significant differences.

3 Results and discussion

The results of the bulk simulations are summarized in Table 1. A minimum of 20 simulations are performed for each system; a maximum of 128 simulations are performed for the $C_{63}N_1$ and $C_{63}B_1$ cases. Note, to simplify our notation, we denoted $C_{63}N_1$ as N1, and similarly for the iron and boron cases. For iron, we denote the constant density simulations as FeX and the constant volume simulations as FeX′. During entry, the surface of the heat shield erodes principally by the loss of atoms, therefore, the cohesive energy, E_c, per atom is expected to be a good measure of the performance of these materials. In Table 1, we reported E_c to illustrate the changes in thermal stability associated with replacing carbon atoms with Fe, B, or N atoms;

$$E_c = (E(C_mX_n) - mE(C) - nE(X))/(n+m)$$

where $E(C_mX_n)$ is the energy of the char with m carbon atoms and n X atoms, and $E(C)$ and $E(X)$ are the ground state energies of the carbon and X atoms, respectively.

At our level of theory, the cohesive energy of diamond is 7.80 eV. This is in good agreement with the experimental value [56] of 7.35 eV. Since we used a functional

Table 1 Summary of the results

System[a]	E_c	% Threefold	% Fourfold	Rho	K
Average bulk					
C	7.35[b]	86.3	7.2	2.000	149 ± 37
N1	7.25	82.7	9.2	2.005	
N2	7.20	83.1	7.8	2.010	
N6	7.07	78.0	7.3	2.031	123 ± 49
N12	6.85	71.5	8.4	2.062	
B1	7.27	82.9	10.0	1.997	
B2	7.26	82.4	11.4	1.995	
B6	7.15	81.7	12.9	1.985	141 ± 43
B12	7.03	77.5	16.6	1.968	
N3B3	7.13	79.5	10.8	2.007	144 ± 40
Fe1	7.16	77.6	6.3	2.000	
Fe2	7.14	75.7	4.5	2.000	
Fe6	6.82	47.7	0.9	2.000	69 ± 25
Fe12	6.48	17.7	0.0	2.000	
Fe1′	7.19	80.4	8.1	2.111	
Fe2′	7.14	78.2	6.3	2.228	
Fe6′	6.91	63.4	3.4	2.684	
Average surface					
C	7.14	77.1	5.8	2.157	
N1	7.06	74.0	7.7	2.151	
N6	6.91	70.8	6.5	2.104	
B1	7.08	73.7	8.4	2.174	
B6	7.01	74.8	10.2	2.145	
Best surface					
C	7.36	84.4	3.1	2.233	
N1	7.23	87.5	1.6	2.321	
B1	7.34	90.6	6.3	2.326	

The per atom cohesive energy, E_c, is in eV and the density, rho, is in g/cm^3. The percent of atoms with 3 or 4 neighbors, that is, threefold or fourfold coordination, is also given. The bulk modulus (K) is given in GPa

[a] The number after the "Fe", "B" or "N" signifies the number of carbon atoms replaced by iron, boron or nitrogen atoms, respectively. FeX is constant density while FeX′ is constant volume

[b] The value for diamond at the same level of theory is 7.80 eV

without exact exchange, it is not surprising that the DFT results are overbound with respect to experiment. Such over binding has been observed in previous work [5, 56]. Our DFT values for amorphous carbon are 0.45 eV smaller than for diamond. This difference is similar to the annealed value of 0.5 eV obtained by Kumagai et al. [15] using the Brenner potential. It is also similar to, but smaller than, the DF-tight binding result (0.6 eV) of Köhler et al. [5] and the tight binding result (0.66 eV, for 2.2 g/cm^3) by Wang and Ho [4]. We expect that our DFT value should be more accurate than these less rigorous methods.

The first thing to note is that replacing carbon atoms with nitrogen, boron, or iron atoms reduces the cohesive energy. The larger the number of dopant atoms added to the carbon, the larger the decrease in cohesive energy. The decrease in cohesive energy with the number of added iron atoms is slightly larger for constant density case (FeX) than for the constant volume case (FeX′). For a given number of added atoms, the decrease in the cohesive energy is the largest for iron and smallest for boron. Adding nitrogen and boron at the same time, the N3B3 case, results in a binding energy that is between N6 and B6 cases, but closer to the more strongly bound boron case. While BN introduces the possibility of an ionic component to the bonding and in 13 out of the 20 simulations at least one B-N bond forms, the introduction of B and N does not translate into increased bonding. While adding nitrogen or boron decreases the binding energy, the effect is small up to the X6 cases; consider the N6 and B6 results, where the decrease per atom is only 0.28 and 0.20 eV, respectively, or as a percentage, the binding energy is 96.2 or 97.2 % of the all carbon case.

We investigate the bonding by counting the number of neighbors for each atom. While using the distance to determine the number of bonds is a simple approach, it should be sufficiently accurate to show the trends. Overall, the changes in the character of the bonding, as measured by the average number of neighbors, are small with the replacement of the carbon atoms by either boron or nitrogen atoms. The small changes in the bonding are consistent with the small changes in the cohesive energy. The percentage of atoms that are threefold coordinated decreases with increasing impurity concentration, excluding N1 to N2, where there is a small increase. This increase could be due to the number of simulations or the simplicity of the bond counting method. The percent of atoms with 4 neighbors decreases with increasing nitrogen concentration for one to six nitrogen atoms, but actually increases between six and 12 nitrogen atoms. In all of our simulations, the nitrogen atoms are threefold coordinated, so the fourfold coordination is only due to the carbon atoms. Clearly, the addition of nitrogen does not significantly change the number of neighbors (hybridization) of the carbon atoms. Somewhat surprising is the fact that the percentage of the atoms with fourfold coordination increases with increasing boron concentration. In our simulations about 15 % of the boron atoms form four bonds; the four bonds presumably form due to carbon donation of electrons into an empty boron 2*p* orbital. A typical structure for the B6 simulations is shown in Fig. 1. There is one fourfold boron atom noted with an arrow. The other boron atoms are threefold coordinated as are a majority of the carbon atoms. Note that the apparently twofold coordinated B atoms are a result of the truncation of the cell. That is, the cells with boron atoms added look very much like those with only carbon atoms.

The change in number of neighbors with the number of added iron atoms is larger than found for nitrogen or boron, especially for the constant density case, where the number of threefold coordinated (sp^2) carbons is less than 50 % for Fe6 and only 17.7 % for Fe12. Inspection of the structures shows that expansion of the cell size to retain the 2.0 g/cm^3 density results in the formation of carbon chains (i.e., some of the carbons have *sp* hybridization) with few interconnections. One of the clearer examples of the chain structure for the 2.0 g/cm^3 simulations is shown in Fig. 2. The large reduction in the cohesive energy is consistent with this change in the structure. For the constant volume iron calculations, the change in the bonding is much less dramatic.

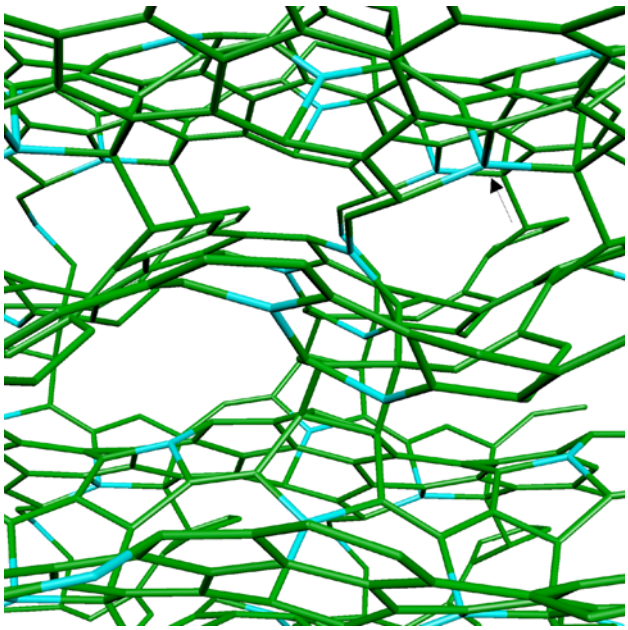

Fig. 1 A typical B6 structure. The carbon atoms are *green* and the boron atoms are *blue*. The bond from the atom to the bond midpoint is the color of that atom. Thus, the bond between two carbon atoms is all *green*, while a bond between a carbon and boron is *half green* and *half blue*. The fourfold boron atom is noted by the *arrow*. The cell contained 64 atoms and periodic boundary conditions are used in this structure

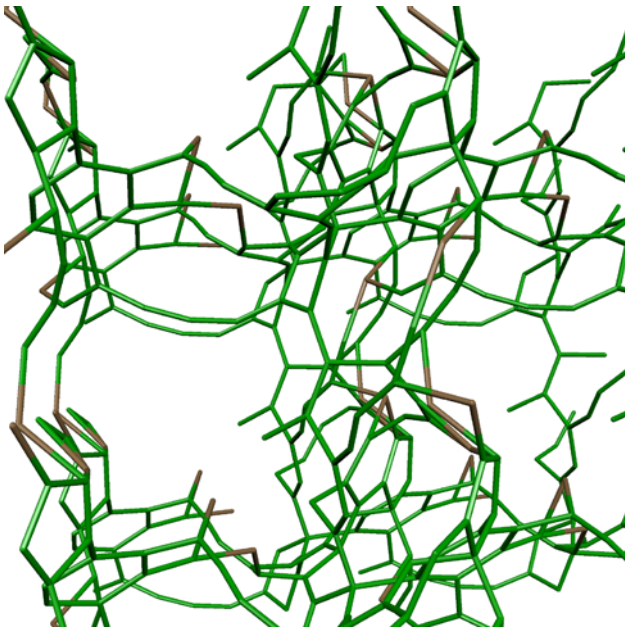

Fig. 2 A typical Fe6 structure. The carbon atoms are *green* and the iron atoms are *brown*. The bond from the atom to the bond midpoint is the color of that atom. Thus, the bond between two carbon atoms is all *green*, while a bond between a carbon and iron is *half green* and *half brown*. Note the formation of carbon chains. The cell contained 64 atoms and periodic boundary conditions are used in this structure

The Fe6′ structures look very much like those for pure carbon, B6, N6, and B3N3. While one observes some chains in the Fe6′ structures, one also observes some chains in the carbon, B6, N6 and B3N3 systems, and it is difficult to determine whether there is an increase in chains in the Fe6′ structures relative to the others. This observation is consistent with the small change in the number of neighbors (hybridization) in the Fe6′ system compared with carbon, B6, N6, and B3N3. Clearly, the Fe6′ and Fe6 systems are quite different.

For the pure carbon, B6, N6, B3N3, and Fe6 cases, we computed the bulk modulus, which are also given in Table 1. Due to the limited number of simulations, there is a non-trivial standard deviation for the values, but it is still possible to draw some conclusions. We first note that the bulk modulus for diamond at this level of theory is 470 GPa and for amorphous carbon with a density of approximately 3 g/cm^3 is 311 ± 67 GPa. From the pure carbon case, it is clear that reducing the density to 2 g/cm^3 has significantly reduced the bulk modulus, with the value being about half that of the 3 g/cm^3 material. Excluding the B3N3 case, adding the impurity atoms has reduced the bulk modulus. The most dramatic effect is for the 2.0 g/cm^3 Fe6 case, where the bulk modulus is less than half the pure carbon case. While the order C > B6 > N6 is consistent with the cohesive energy, the C ≈B3N3 is a bit unexpected. If more simulations were performed, it is possible that the B3N3 value would fall between the B6 and N6 results. The alternative is that the ionic component of the bonding in B3N3 contributes to increasing the bulk modulus (a mechanical property), but does not lead to increased thermal stability. It is possible that the bulk modulus correlates better with the heat of formation, but before making such a comparison, additional simulations should be performed to reduce the error bars, which is beyond the scope of this work. We should note that Merchant et al. [26] computed the bulk modulus for amorphous carbon nitrides and found a reduction in K with decreasing density, namely 336, 295, and 273 GPa for 3.2, 2.95, and 2.45 g/cm^3, respectively. Our value for 3 g/cm^3 pure carbon is consistent with their values for 3.2 and 2.95 g/cm^3, and our value for 2 g/cm^3 shows that the rate of decrease in K with decreasing density may even accelerate as the density reaches 2 g/cm^3.

In Fig. 3, we plot the absorbance and reflectivity for the pure carbon and the doped cases over the range 0–20 eV. The results are the average of all simulations. The bottom curves are for pure carbon; the carbon absorbance curve is well understood. The 5 eV peak is associated with the $\pi \rightarrow \pi^*$ transition, while the 15 eV peak is associated with the $\sigma \rightarrow \sigma^*$ transition. Above the carbon curves are the curves for N, B, and Fe as a function of concentration. For nitrogen and boron, the most notable feature of the figures is the relatively small changes in absorption with changing concentration. These small changes are consistent with the small change in the number of neighbors (hybridization) shown in Table 1. The change in the absorption with increasing Fe concentration is much larger, which is consistent with the much larger changes in hybridization, bonding, and volume. The reflectivity shows the same trends with changing species as does the absorbance. Namely, the addition of iron results in much larger changes than do the addition of nitrogen or boron. The similarity of the absorbance and reflectivity is not unexpected as they are both computed from the dielectric function.

To allow an easier comparison of the different dopants, the six dopant atom absorbance cases, that is, X6, along with the pure carbon, are plotted in Fig. 4. Clearly, the results for the pure carbon, B6, N6, and B3N3 are all very similar, while those for Fe6 and Fe6′ are different from the others. The same is true for the reflectivity (not shown). The Fe6 has similar peak positions as the others, but the height of the peaks is quite different. The absorbance shows that the Fe6′, which has the same volume as B6, N6, and B3N3, is similar to those for pure carbon, B6, N6, and B3N3 from about 7–20 eV. That is, the difference between Fe6 and the other curves in this region is due to the larger volume. From 0 to about 7 eV, the Fe6′ differs from the other systems by somewhat more than the Fe6 case. That Fe6′ increases the peak associated with $\pi \rightarrow \pi^*$ is perhaps a

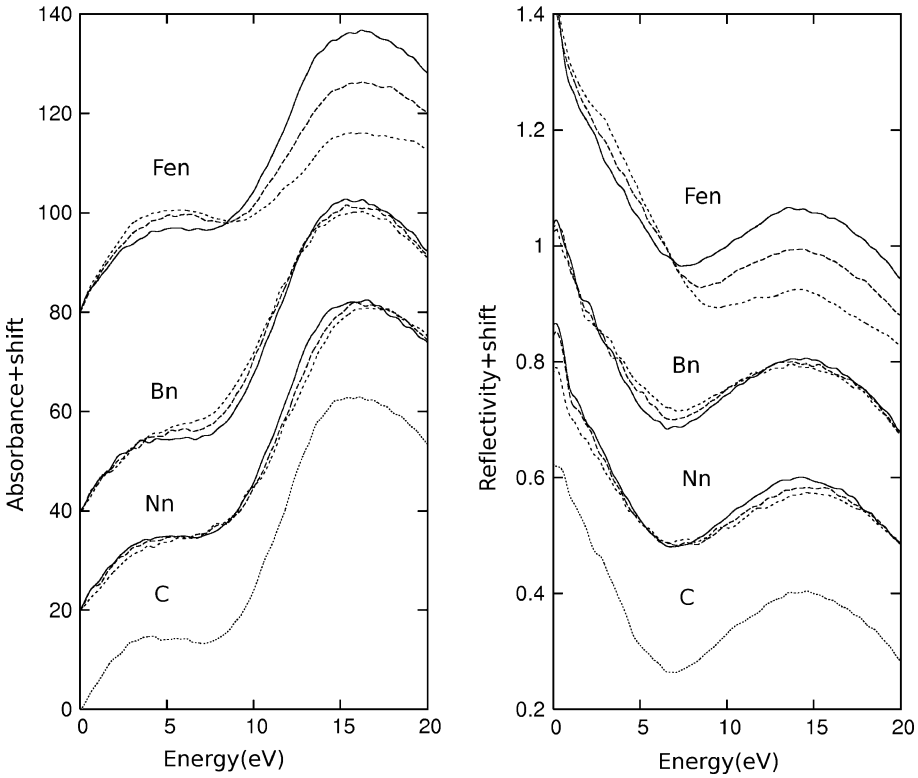

Fig. 3 The optical properties (absorbance and reflectivity) versus energy. The absorbance curves have been shifted by 20, 40, and 80 for N, B, and Fe, respectively. The reflectivity curves have been shifted by 0.2, 0.4, and 0.7 for N, B, and Fe, respectively. The pure carbon is a *dotted line*, the X2 is the *solid line*, the X6 is the *long dashed line* and the X12 is the *short dashed line*

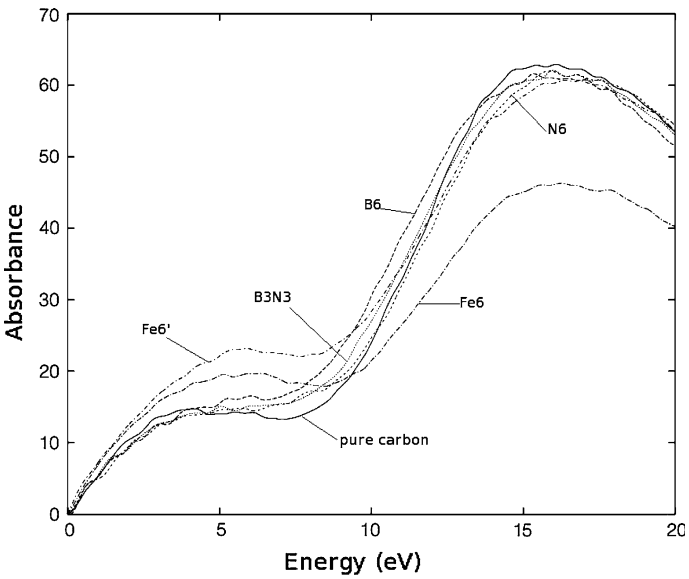

Fig. 4 Comparison of the absorbance versus energy for Fe6 (constant density), Fe6′ (constant volume), B6, N6, B3N3, and pure carbon

bit surprising considering the similarities in hybridization for Fe6′, carbon, B6, N6, and B3N3. Finally, we note that in the 15 eV region, both the absorbance and reflectivity decrease for Fe6, hence the transmission increases, probably because of more empty space in the cell.

On the basis of the small changes in the absorbance and reflectivity with the addition of boron and/or nitrogen atoms, we conclude that replacing carbon atoms with either boron or nitrogen atoms will not significantly effect the impact of radiative heating. For the 2.0 g/cm^3 iron dopant case, the change in optical response depends on the energy. For energies below about 7 eV, the iron increases absorption, but also increases reflectivity, thus the transmission is decreased. The increased reflectivity means that overall heating would be reduced, but the increased absorption and decreased transmission means that the surface would absorb more energy, but the subsurface heating would be reduced. Above 7 eV, the iron reduces the reflectivity and

hence increases the overall heating; however, changes in the absorption and transmission mean that the heating is spread over more of the heat shield. Clearly, detailed knowledge of the shock spectra is require to see whether adding iron would affect the optical response, however, we note that for a lunar return about 60 % of the energy is below 4 eV, and therefore, iron might be important for some entries and additional work is probably warranted.

The site-projected DOS, which are averaged over all simulations, (Fig. 5) provide additional insight into the changes associated with the addition of Fe. The bottom curve shows site-projected DOS for pure carbon. The carbon DOS does not show much structure. This is caused by the nature of the bonding in these low-density amorphous structures where bonds are stretched or compressed and angles bend away from the optimal values. Averaging of the different structures further increases the variation in the bonding that leads to the lack of structure in the DOS. The next plot shows the B6 case. The site-projected carbon curve looks like the pure carbon case, while the site project boron DOS values are very small at the low energies (below the region shown in the figure), rising to a small value that shows some variation in the valence region; that is, the boron and carbon site-projected DOS curves appear similar, but with the boron curve being much smaller than carbon curve. Since boron values are much smaller than the carbon values, its site-projected DOS appears essentially flat on the scale of these plots. Clearly, the boron at this concentration does not significantly alter the DOS. We should note that the boron values are smaller than expected based on the number of electrons, and this is due to the Bader approach used to determine the atomic volumes. If Voronoi polyhedra are used instead of Bader to determine the atomic volumes, the boron population increases as does the site-projected DOS values, but the site-projected DOS curve looks very much like that obtained from the Bader approach. Like the B6 case, the N6 and B3N3 curves show little structure and are not shown. Unlike the boron, the addition of Fe changes the DOS. The site-projected DOS shows that the Fe can be even more important than carbon for some energies even though only about 10 % of the atoms are iron. Clearly, the increase in the absorbance in 0–7 eV range appears to involve Fe atoms. A careful comparison of the Fe6 results with the others shows that there are several regions where there are some additional differences, which probably arise from the formation of more chains.

As noted in the introduction, previous work for higher density systems showed an increase in the 5 eV peak in the absorbance curve with the addition of boron or nitrogen. This has been interpreted as arising from the formation of extended π bonding, that is, the isolated π bonds in the all carbon system migrate together when the impurity atoms are present. However, for the low-density all carbon system, the situation is rather different. In the pure carbon 2.0 g/cm^3, the average number of atoms included in the

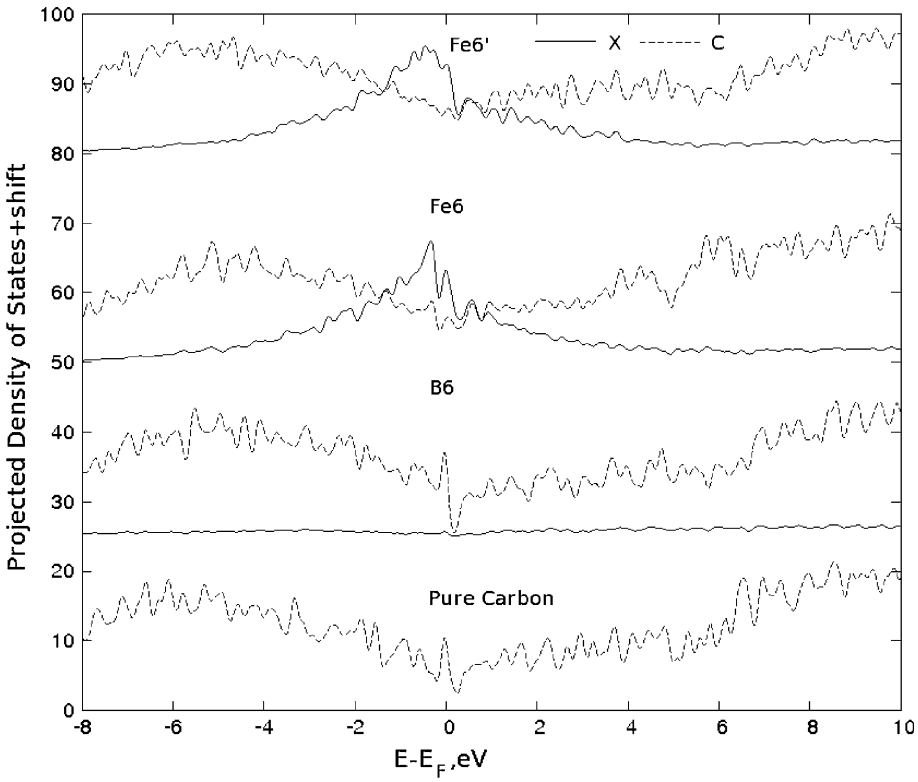

Fig. 5 The site-projected DOS for pure carbon, B6, Fe6, and Fe6′. The B6, Fe6, and Fe6′ curves have been shifted. The Fermi energy, E_F, has been subtracted from the energy

extended π bonded network is 59.4 for the 20 simulations considered in this work. The analogous values for B6 and N6 are 55.7 and 58.6 atoms, respectively. In one B6 simulation, a two atom pi bond formed and in a few of the N6 simulations two and four atom pi bonded cluster formed. This is opposite to the effect noted in the higher density cases. Given that adding B or N does not significantly alter the size of the pi bonded cluster of atoms, it is not surprising that they do not change the absorbance significantly. The analogous values for Fe6 and Fe6′ are 60.1 and 58.3, respectively. Thus, Fe is not changing the size of the pi bonded cluster, however, as noted above some pi bonded clusters involve *sp* not sp^2 hybridization. The largest changes with the addition of iron appear to be due to the partly filled Fe 3d orbital that changes the DOS states near the Fermi level.

Table 1 reports the results of the simulations of the surfaces. Because of the larger reduction in the cohesive energy for iron, we do not consider surfaces with iron added. These surface simulations start from 20 carbon bulk simulations, 64 bulk simulations for both N1 and B1, and 20 bulk simulations for both N6 and B6. The x, y, and z directions are all considered as surface, leading to 60 carbon surface simulations, 192 surface simulations for both N1 and B1, and 60 surface simulations for both N6 and B6. As we noted in previous work [1], some of the surface simulations become nonphysical. The two most common problems are the formation of a chain of atoms with one end attached to the surface or the formation of a sheet of atoms that is either unbound or bound to the rest of the atoms by a chain of atoms. For the N6 simulations, the formation of CN groups sticking out of the surface is quite common. In addition, for some of the N6 simulations, N_2 forms and leaves the surface. All of these cases are easily detected because they have low densities. In this work, we reject any surface simulation with a density of less than 1.9 g/cm^3. The number of rejected simulations is 25 for B1, 24 for N1 and 6 for the all carbon; a little more than 10 % of the simulations are rejected. The B6 simulations show 9 runs rejected out 60, which is 15 %, a bit higher than for the C, N1, and B1 simulations. The N6 simulations are distinctly different, where 25 out of 60 runs are rejected.

As can be seen in Table 1, the addition of nitrogen or boron to the surface reduces the atomization energy. The decrease is larger for the X6 cases than the X1 cases, with the loss in binding energy for the N6 case being very noticeable. Formation of N_2 and the number of rejected simulations for the N6 case also supports the idea that adding 6 nitrogen atoms destabilizes the surface greatly. Because of the sizable variation in the atomization energy among simulations of the same surface, we consider the best surface energy for pure carbon and the N1 and B1 simulations, and find adding B or N still destabilizes the surface.

4 Conclusions

We have considered replacing up to almost 20 % of the carbon atoms in 2.0 g/cm^3 amorphous carbon by iron, nitrogen, or boron atoms. We find that this replacement of carbon reduces the cohesive energy and the decrease becomes larger with increasing concentration of the Fe, B, or N atoms. The reduction in cohesive energy is largest for Fe and smallest for B. The results for adding $(BN)_n$ fall between those for B_{2n} and N_{2n}. The calculation of the reflectivity and absorbance does not show significant difference between the 100 % carbon models and those with B and/or N added. This result is different from higher density amorphous carbon systems where the addition of B and N increases the absorption by causing isolated sp^2 carbons to form extended networks. This does not occur for the lower density amorphous cases since extended networks of sp^2 carbons are already present. Adding Fe changes the structure more and hence the absorbance and reflectivity change by more than that found for N or B. At low iron concentration, these differences arise from the chemical properties of the iron atom, while at higher iron concentrations, the constant density simulations show some changes come from the larger volume resulting from the larger atomic mass of the iron atoms. The effect of adding iron depends on the shock emission spectra and hence on the specific entry. Our work is consistent with the limited number of previous bulk simulations, and we look forward to confirmation of our predictions by experiments on low-density materials.

Simulations of the surfaces are consistent with those of the bulk, showing that the addition of B and N reduce the atomization energy of the surface. This work shows that adding either boron or nitrogen to heat shield char will not significantly affect its bulk or surface strength nor change its optical absorption properties. The loss in cohesive energy is much larger for Fe than either B or N, suggesting Fe will degrade the performance of a thermal protection system. However, the optical properties also change with the addition of iron, and for some entries, the change in optical properties might be beneficial.

References

1. Bauschlicher CW, Lawson JW (2010) Chem Phys 374:77–82
2. Galli G, Martin RM, Carr R, Parrinello M (1989) Phys Rev Lett 62:555
3. Galli G, Martin RM, Carr R, Parrinello M (1990) Phys Rev B 42:7470
4. Wang CZ, Ho KM (1994) Phys Rev B 50:12429
5. Köhler Th, Frauenheim Th, Jungnickel G (1995) Phys Rev B 52:11837
6. Marks NA, McKenzie DR, Pailthorpe BA, Bernasconi M, Parrinello M (1996) Phys Rev Lett 76:768

7. Marks NA, McKenzie DR, Pailthorpe BA, Bernasconi M, Parrinello M (1996) Phys Rev B 54:9703
8. De Vita A, Galli G, Canning A, Carr R (1996) Nature 379:523
9. Dong J, Drabold DA (1998) Phys Rev B 57:15591
10. Marks NA, Cooper NC, McKenzie DR, McCulloch DG, Bath P, Russo SP (2002) Phys Rev B 65:075411
11. Robertson J (2002) Mat Sci Eng R 37:129
12. Petersen T, Yarosky I, Snook I, McCulloch DG, Opletal G (2004) Carbon 42:2457
13. Lawson JW, Srivastava D (2008) Phys Rev B 77:144209
14. Makeev MA, Srivastava D (2010) J Chem Phys C 114:5709
15. Kumagai T, Choi J, Izumi S, Kato T (2010) J Appl Phys 107: 104307
16. McKenzie DR (1996) Rep Prog Phys 59:1611
17. Wan C, Zhang X, Zang X, Gao X, Tan X (2009) App Phys Lett 95:022105
18. Yastrebov SG, Ivanov-Omskii VI, Kosobukin VA, Dumitrache F, Morosanu C (2004) Tech Phys Lett 30:995
19. Chen JS, Lau SP, Chen GY, Sun Z, Li YJ, Tay BK, Chai JW (2001) Diam Rel Mat 10:2018
20. Chen JS, Lau SP, Tay BK, Chen GY, Sun Z, Tan YY, Tan G (2001) J Appl Phys 89:7814
21. Xiong Y, Xie Y, Li X, Li Z (2004) Carbon 42:1447
22. Weich F, Widany J, Frauenheim Th (1997) Phys Rev Lett 78:3326
23. Chen CW, Robertson J (1999) Carbon 37:839
24. Lenardi C, Piseri P, Briois V, Bottani CE, Li Bassi A, Milani P (1999) J Appl Phys 85:7159
25. Waidmann S, Knupfer M, Fink J, Kleinsorge B, Robertson J (2001) J Appl Phys 89:3783
26. Merchant AR, McKenzie DR, McCulloch DG (2001) Phys Rev B 65:024208
27. Zhang XW, Cheung WY, Ke N, Wong SP (2002) J Appl Phys 92:1242
28. Messasalma AM, Mondio G, Neri F, Trusso S (2003) J Phys D 36:541
29. Ferrari AC, Rodil SE, Robertson J (2003) Phys Rev B 67:155306
30. de Sánchez N Alba, Carrosco C, Prieto P (2003) Phys B 337:318
31. Rodil SE, Muhl S (2004) Diam Rel Mat 13:1521
32. Wang XC, Wu P, Li ZQ, Jiang EY, Bai HL (2004) J Phys D 37:2127
33. Houska J, Bilek MMM, Warschkow O, McKenzie DR, Vlcek J (2005) Phys Rev B 72:054204
34. Titantah JT, Lamoen D (2006) Phys Stat Sol A 203:3191
35. Valladares AA, Álvare-Ramírez F (2006) Phys Rev B 73:024206
36. Abrasonis G, Gago G, Vinnichenko M, Kreissig U, Kolitsch A, Möller W (2006) Phys Rev B 73:125427
37. Titantah JT, Lamoen D (2007) Diam Rel Mat 16:581
38. Han J, Gao W, Zhu J, Meng S, Zheng W (2007) Phys Rev B 75:155418
39. Lau DWM, McCulloch DG, Taylor MB, Partridge JG, McKenzie DR, Marks NA, Teo EHT, Tay BK (2008) Phys Rev Lett 100:176101
40. Kleinsorge B, Ilie A, Chhowalla M, Fukarek W, Milne WI, Robertson J (1998) Diam Rel Mat 7:472
41. Gambirasio A, Bernasconi M (1999) Phys Rev B 60:12007
42. Dai Y, Yan Y, Wang J, Sun B, He X, Shen H (2005) J Appl Phys 98:013525
43. Tan M, Zhu J, Han J, Gao W, Niu L, Lu J (2007) Diam Rel Mat 16:1739
44. Tan M, Zhu J, Han J, Gao W, Liu A, Han X (2008) Mat Res Bull 43:453
45. Sikora A, Berkesse A, Bourgeois O, Garden J-L, Guerret-Piécourt C, Rouzaud J-N, Loir A-S, Garrelie G, Donnet C (2009) Solid State Sci 11:1738
46. Kalijadis A, Jovanović Z, Laušević M, Laušević Z (2011) Carbon 49:2671
47. Gajdōs M, Hummer K, Kresse G, Furthmüller J, Bechstedt F (2006) Phys Rev B 73:045112
48. Baroni S, Resta R (1986) Phys Rev B 33:7017
49. Henkelman G, Arnaldsson A, Jónsson H (2006) Comput Mat Sci 36:354
50. Kresse G, Hafner J (1993) Phys Rev B 47:558
51. Kresse G, Hafner J (1994) Phys Rev B 49:14251
52. Kresse G, Furthmüller J (1996) Comput Mat Sci 6:15
53. Kresse G, Furthmüller J (1996) Phys Rev B 54:11169
54. Perdew JP, Wang Y (1991) Phys Rev B 45:13244
55. Kresse G, Joubert J (1999) Phys Rev B 59:1758
56. Yin MT, Cohen ML (1984) Phys Rev B 29:6996